Ni_3Sn_4 Electrodes for Li-Ion Batteries: Li−Sn Alloying Process and Electrode/Electrolyte Interface Phenomena

K. K. D. Ehinon,[†] S. Naille,[‡] R. Dedryvère,*[,†] P.-E. Lippens,[‡] J.-C. Jumas,[‡] and D. Gonbeau[†]

IPREM/ECP, Université de Pau, Hélioparc Pau Pyrénées, 2 av. Pierre Angot, 64053 Pau cedex 9, France, and Institut Charles Gerhardt, AIME, UMR CNRS 5253, Université Montpellier II, Place E. Bataillon, CC1501, 34095 Montpellier cedex 5, France

Received March 3, 2008. Revised Manuscript Received May 21, 2008

We have investigated the reaction mechanisms of lithium toward Ni_3Sn_4 in an electrochemical cell and the electrode/electrolyte interface phenomena in a combined X-ray photoelectron spectroscopy (XPS) and ^{119}Sn Mössbauer spectroscopy approach, which allows a simultaneous analysis of the surface and of the bulk of the active material particles. We show that 4 mol of lithium per mole of Ni_3Sn_4 are consumed to form the solid electrolyte interface (SEI) at the first stage of discharge. The composition and behavior of this SEI have been compared to those observed with graphite. The Li−Sn alloying process occurs in the second stage of discharge to form Li_7Sn_2. This mechanism is reversible and allows restoring the Ni_3Sn_4 phase at the end of the cycle.

1. Introduction

In the majority of the marketed Li-ion batteries, the negative electrode is made up of carbon. The theoretical specific capacity of a graphite electrode is 372 (mA h)/g (833 (mA h)/cm^3). However, the capacity remains limited to 300−330 (mA h)/g during cycling. During the first lithium intercalation, the graphite electrode is covered by a passivating layer called the "solid electrolyte interphase", SEI [1,2] which is formed by reaction of the electrode surface with the electrolyte. The formation of this layer, associated to the reduction of electrolytic species (i.e., salts, solvents), results in a loss of capacity. Nevertheless, this passivating surface layer is stable for graphite, protects the electrode, and prevents further degradation of the electrolyte during the following cycles. Therefore, SEI supports the migration of lithium ions and thus a good behavior upon cycling.[2]

Presently, numerous materials are studied as alternatives to carbon electrodes. These new materials should fulfill several criteria, particularly a considerable increase of their energy densities, in order to replace carbon as anodic materials in new applications. One of the research orientations during the last years has been the study of pure elements, such as metals alloying with lithium.

In 1971 Dey showed the possibility to form lithium−metal alloys via electrochemical reactions in an organic electrolyte with a reversible process:[3]

$$M + xLi^+ + xe^- \underset{\text{discharge}}{\overset{\text{charge}}{\rightleftharpoons}} Li_xM \quad (1)$$

He showed that lithium−metal alloys were formed at room temperature, even when the Li−M binary phase diagram was complex. The electrochemical reaction between lithium ions and metal occurs in several stages, with the successive formation of stoichiometric intermetallic compounds and intermediate phases of the associated binary system. In particular, this process is characterized by the appearance of several plateaus on the electrochemical curve.

In this respect, tin is as an attractive element for such reactions. Indeed, it can form up to seven alloys with different compositions: Li_2Sn_5, LiSn, Li_7Sn_3, Li_5Sn_2, $Li_{13}Sn_5$, Li_7Sn_2, and $Li_{22}Sn_5$.[4−6] The formation of the different Li_xSn alloys is achieved with potentials ranging between 0.66 and 0.38 V versus Li^+/Li^0 at room temperature, which is well-suited for their use as negative electrodes.[7] Indeed, despite a resulting lower cell voltage, a higher electrode potential as compared to lithiated graphite (0.1−0.2 V vs Li^+/Li^0) reduces the reactivity of the material and the risks of metallic lithium deposition during rapid charge.

Lithium can alloy with tin up to a maximum composition, namely, $Li_{22}Sn_5$ ($Li_{4.4}Sn$), which corresponds to a theoretical specific capacity of 993 (mA h)/g (7229 (mA h)/cm^3), definitely higher than those reached with carbon. However, for all pure metals being able to alloy with lithium, the reaction is accompanied by a severe volume variation, which produces high mechanical strains. These strains cause a rapid

* Corresponding author. E-mail: remi.dedryvere@univ-pau.fr.
[†] Université de Pau.
[‡] Université Montpellier II.

(1) Peled, E. *J. Electrochem. Soc.* **1979**, *126*, 2047.
(2) Peled, E.; Golodnitsky, D. In *Lithium-Ion Batteries: Solid-Electrolyte Interphase*, Balbuena, P. B., Wang Y., Eds.; Imperial College Press: London, 2004.
(3) Dey, A. N. *J. Electrochem. Soc.* **1971**, *118*, 1547.
(4) Wen, C. J.; Huggins, R. A. *J. Electrochem. Soc.* **1981**, *128*, 1181.
(5) Wang, J.; Raistrick, I. D.; Huggins, R. A.; Besenhard, J. O. *Electrochem. Solid-State Lett.* **1999**, *2*, 161.
(6) Robert, F.; Lippens, P.-E.; Olivier-Fourcade, J.; Jumas, J.-C.; Gillot, F.; Morcrette, M.; Tarascon, J.-M. *J. Solid State Chem.* **2007**, *180*, 339–348.
(7) Wang, J.; Raistrick, I. D.; Huggins, R. A. *J. Electrochem. Soc.* **1986**, *133*, 457.

10.1021/cm8006099 CCC: $40.75
Published on Web 07/01/2008

fading of the mechanical properties of the electrode and thus its destruction.[8,9] This severe volume change is therefore one of the most important issues for the loss of capacity of electrodes containing pure metals. In the case of tin, this volume expansion is 257% when the $Li_{22}Sn_5$ alloy is formed.

Several strategies, including the use of Sn-based intermetallics, were considered to minimize these volume variations and obtain good cycling behaviors. The principal idea in the use of Sn-based intermetallics rather than pure tin is that, at a certain stage of the charge (i.e., at a given potential), tin is able to react with lithium (i.e., to form Li_xSn alloys) whereas the other metal is electrochemically inactive (i.e., plays the role of a "matrix" buffering the volume expansion).[8] The other metal is generally a transition metal.

Various Sn-based intermetallic compounds have been investigated by several research groups and tested as possible negative electrode materials. Among the recently studied systems, we can cite Cu_6Sn_5, $MnSn_2$, $FeSn_2$, $CoSn_2$, or Ni_3Sn_2.[10–15] All these systems present high capacities compared to those of graphite. Ni_3Sn_4 was also investigated by several groups.[16,17] However, despite a remarkable specific capacity during the first discharge, the capacity retention of these intermetallics is not satisfactory upon prolonged cycling. So far, the only mechanism that has been proposed for Ni_3Sn_4 to explain its reaction with lithium ions is the following:[18] during the first electrochemical discharge, Ni_3Sn_4 reacts with lithium to form the lithium-richest alloy $Li_{4.4}Sn$ ($Li_{22}Sn_5$), with the separation of nickel:

$$Ni_3Sn_4 + 17.6Li^+ + 17.6e^- \rightarrow 3Ni + 4Li_{4.4}Sn \qquad (2)$$

This process is not reversible upon charge, and it is replaced by the following reversible mechanism, which also takes place during the following electrochemical cycles:

$$Li_{4.4}Sn \leftrightarrow Sn + 4.4Li^+ + 4.4e^- \qquad (3)$$

In the present paper, we will discuss mechanisms 2 and 3 and propose an alternative to describe the reactivity of Ni_3Sn_4 toward lithium.

Several processes are responsible for the high irreversible capacity of intermetallics, such as the loss of electronic contact between electrode particles due to volume variations, the reduction of oxide impurities, or the formation of solid electrolyte interphase (SEI) at the surface of the electrode. SEI phenomena on intermetallics have not been studied as thoroughly as for graphite. Wachtler et al. have displayed specific problems due to intermetallic electrodes as compared to graphite.[9] The surface of the active material undergoes a continuous reconstruction, due to considerable volume changes of the lithium alloy particles upon charge and discharge. The SEI has thus to follow the changes of the surface, its continuous formation may consume a large amount of lithium and electrolyte components, and consequently it may strongly contribute to the irreversible capacity. Rather few studies have been devoted to the formation mechanisms and to the composition of the SEI at the surface of intermetallic electrodes.[19,20] The composition of this layer is expected to be rather similar to that observed for graphite, but its thickness is supposed to be greater, due to the morphological changes of the electrode.[2] Recently, Edström and co-workers[21] have shown that the SEI at the surface of AlSb electrodes mainly consists of the same species found for graphite, including LiF and carbonate species (i.e., Li_2CO_3 and $ROCO_2Li$). However, they found that the thickness of the SEI increases during lithiation and decreases during delithiation. In particular, after 50 cycles the SEI is thinner than for graphite, contrary to expectation. Simultaneously, we also showed that the SEI at the surface of Cu_6Sn_5 electrodes mainly consists of LiF and carbonate species but that its thickness is stable during the whole electrochemical cycle.[22]

In this work, we will investigate the Li−Sn alloying process occurring upon lithiation/ delithiation of Ni_3Sn_4 electrodes in a combined X-ray photoelectron spectroscopy (XPS) and ^{119}Sn Mössbauer spectroscopy approach, which allows a simultaneous analysis of the surface and of the bulk of the active particles. A careful investigation of the SEI formation process and its composition has been also carried out via XPS.

2. Experimental Section

2.1. Synthesis. Elemental nickel (Merck, 99.5%, −1250 mesh) and tin (Aldrich, 99%, −1250 mesh) powders were weighed in stoichiometric ratio and mechanically milled for 10 min in a Pulverisette-7 planetary micromill with agate balls and vials under argon atmosphere. The mechanically alloyed powder was placed in an alumina crucible and fired 4 h at 500 °C in a tube-type furnace under a controlled Ar/H_2 (5%) atmosphere to obtain a single-phase and well-crystallized intermetallic.

2.2. Electrochemical Measurements. Electrochemical lithium insertion/extraction tests were performed in Swagelok-type cells assembled in an argon-filled glovebox. Positive electrodes were prepared by mixing 90 wt % pristine powder, 5 wt % carbon black, and 5 wt % polytetrafluoroethylene (PTFE) binder and pressed in 7 mm diameter pellets. Metallic lithium was used as reference and counter electrodes. The electrolyte was 1 M $LiPF_6$ in ethylene carbonate (EC)/propylene carbonate (PC)/dimethyl carbonate (DMC) (1:1:3 v/v/v). The lithium insertion/extraction experiments were

(8) Winter, M.; Besenhard, J. O. *Electrochim. Acta* **1999**, *45*, 31.
(9) Wachtler, M.; Besenhard, J. O.; Winter, M. *J. Power Sources* **2001**, *94*, 189–193.
(10) Larcher, D.; Beaulieu, L. Y.; MacNeil, D. D.; Dahn, J. R. *J. Electrochem. Soc.* **2000**, *147*, 1658–1662.
(11) Choi, W.; Lee, J. Y.; Lim, H. S. *Electrochem. Commun.* **2004**, *6*, 816–820.
(12) Beaulieu, L. Y.; Dahn, J. R. *J. Electrochem. Soc.* **2000**, *147*, 3237.
(13) Mao, O.; Dunlap, R. A.; Courtney, I. A.; Dahn, J. R. *J. Electrochem. Soc.* **1998**, *145*, 4195.
(14) Ionica-Bousquet, C. M.; Lippens, P.-E.; Aldon, L.; Olivier-Fourcade, J.; Jumas, J.-C. *Chem. Mater.* **2006**, *18*, 6442.
(15) Ehrlich, G. M.; Durand, C.; Chen, X.; Hugener, T. A.; Spiess, F.; Suib, S. L. *J. Electrochem. Soc.* **2000**, *147*, 886–891.
(16) Lee, H.-Y.; Jang, S.-W.; Lee, S.-M.; Lee, S.-J.; Baik, H.-K. *J. Power Sources* **2002**, *112*, 8–12.
(17) Cheng, X.-Q.; Shi, P.-F. *J. Alloys Compd.* **2005**, *391*, 241–244.
(18) Amadei, I.; Panero, S.; Scrosati, B.; Cocco, G.; Schiffini, L. *J. Power Sources* **2005**, *143*, 227–230.
(19) Ulus, A.; Rosenberg, Y.; Burstein, L.; Peled, E. *J. Electrochem. Soc.* **2002**, *149*, A635–A643.
(20) Stjerndahl, M.; Bryngelsson, H.; Gustafsson, T.; Vaughey, J. T.; Thackeray, M. M.; Edström, K. *Electrochim. Acta* **2007**, *52*, 4947–4955.
(21) Bryngelsson, H.; Stjerndahl, M.; Gustafsson, T.; Edström, K. *J. Power Sources* **2007**, *174*, 970–975.
(22) Naille, S.; Dedryvère, R.; Martinez, H.; Leroy, S.; Lippens, P.-E.; Jumas, J.-C.; Gonbeau, D. *J. Power Sources* **2007**, *174*, 1086–1090.

performed galvanostatically, using a Mac Pile II system, at a rate of 1 Li/20 h (C/20) within a voltage window of 0.0−1.5 V. The lithiated samples were subsequently recovered in an argon-filled dry box, washed in DMC, and dried under vacuum before characterization.

2.3. X-ray Diffraction (XRD) and Scanning Electron Microscopy (SEM). XRD was performed with a Philips $\theta-2\theta$ diffractometer using Cu Kα radiation ($\lambda = 1.5418$ Å) and a nickel filter, in order to identify phases and check the purity of the samples. Data points were recorded in continuous mode for 2θ angles ranging from 10° to 70°. The powdered sample was observed by scanning electron microscopy (SEM) in order to characterize both the sample morphology and the particle size.

2.4. ^{119}Sn Mössbauer Spectroscopy. ^{119}Sn Mössbauer spectroscopy measurements were carried out at room temperature with a classical EG&G constant acceleration spectrometer using a $Ca^{119m}SnO_3$ γ-ray source. Both transmission Mössbauer spectroscopy (TMS) and conversion electron Mössbauer spectroscopy (CEMS) measurements were performed for the pristine Ni_3Sn_4 material, in order to probe the bulk and the surface (for CEMS, the analysis depth is several hundred nanometers) of the sample, respectively. For CEMS, a gas flow (94% He, 6% methane) proportional counter was used to detect the internal conversion electrons emitted after resonant absorption of γ-rays. Electrochemically lithiated samples were analyzed ex situ by TMS. The electrode materials containing the active particles were placed on a specific sample holder transparent for γ-rays to avoid contact with air. The velocity scale was calibrated using the magnetic sextet spectrum of a high-purity iron foil absorber and ^{57}Co(Rh) as the source. The isomer shifts are given relative to $BaSnO_3$ which is used as the standard reference. All spectra were fit with Lorentzian profiles, by the least-squares method, and the quality of the fit was controlled by the usual χ^2 test.

2.5. XPS. XPS measurements were carried out with a Kratos Axis Ultra spectrometer, using a focused monochromatized Al Kα radiation ($h\nu = 1486.6$ eV). The XPS spectrometer was directly connected through a transfer chamber to a nitrogen dry box, in order to avoid moisture/air exposure of the samples. For the Ag $3d_{5/2}$ line the full width at half-maximum (fwhm) was 0.58 eV under the recording conditions. The analyzed area of the samples was $300 \times 700\ \mu m^2$. Peaks were recorded with a constant pass energy of 20 eV. The pressure in the analysis chamber was around 5×10^{-7} Pa. Short acquisition time spectra were recorded at the beginning and at the end of each experiment to check that the samples did not suffer from degradation during the measurements. The binding energy scale was calibrated from the carbon contamination using the C 1s peak at 285.0 eV. Core peaks were analyzed using a nonlinear Shirley-type background.[23] The peak positions and areas were optimized by a weighted least-squares fitting method using 70% Gaussian, 30% Lorentzian lineshapes. Quantification was performed on the basis of Scofield's relative sensitivity factors.[24]

3. Results and Discussion

3.1. Characterization of Ni_3Sn_4. The synthesized Ni_3Sn_4 material was identified as a single phase compound. XRD analysis (not shown here, see ref 25) allowed the monoclinic structure of Ni_3Sn_4 (*C*2/*m* space group) with $a = 12.187$ (13) Å, $b = 4.055$ (5) Å, $c = 5.216$ (7) Å, and $\beta = 105.19$ (5)°, to be confirmed, in good agreement with data reported in the literature.[26] SEM images revealed a particle size of about 5−20 μm, as shown in Figure 1.

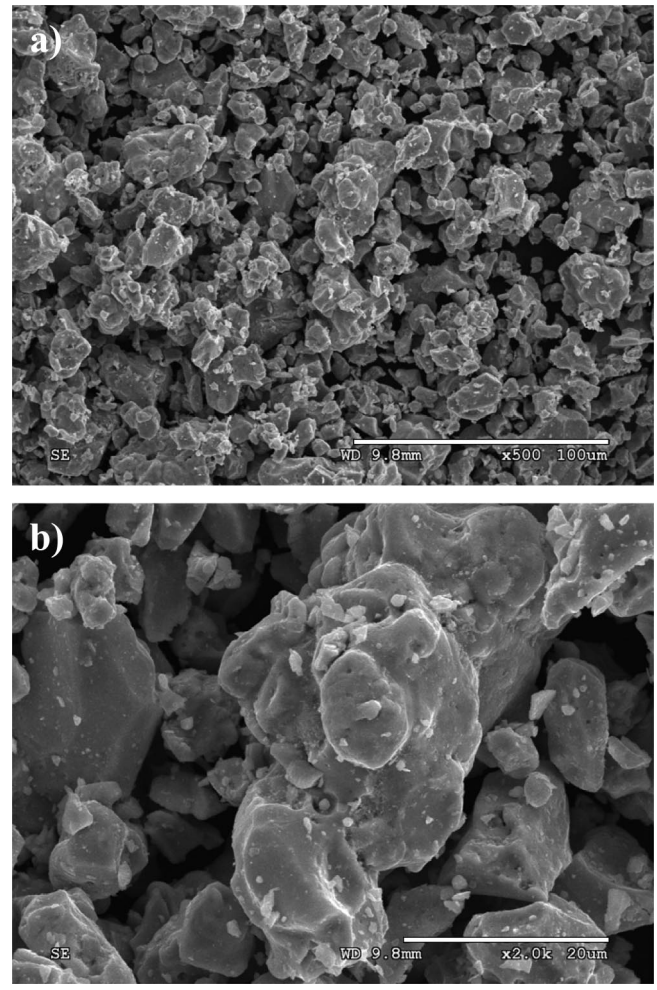

Figure 1. SEM images of the Ni_3Sn_4 powder. Scale: (a) 100 μm, (b) 20 μm (horizontal bar).

Figure 2 shows ^{119}Sn Mössbauer spectra of Ni_3Sn_4 obtained with TMS and CEMS. The relevant hyperfine parameters are reported in Table 1. The transmission Mössbauer spectrum of Ni_3Sn_4 consists of two doublets with equal relative intensity, in good agreement with the crystallographic structure of this compound[26] and with LAPW calculations reported in previous papers.[27,28] Indeed, Sn atoms are located in two different 4i sites of the *C*2/*m* space group with distorted environments. The highest value of quadrupole splitting (Δ) corresponds to a fivefold coordinated site and the other one to a sixfold coordinated site.

The conversion electron Mössbauer spectrum (CEMS) of Ni_3Sn_4 shows, besides the two doublets discussed above, an additional singlet at −0.06 mm/s assigned to SnO_2 with a relative area of 4%. Since CEMS allows a higher surface sensitivity, this result displays the partial oxidation of the surface of the particles. Furthermore, no trace of oxidation

(23) Shirley, D. A. *Phys. Rev. B* **1972**, *5*, 4709.
(24) Scofield, J. H. *J. Electron Spectrosc. Relat. Phenom.* **1976**, *8*, 129–137.
(25) Naille, S.; Ionica-Bousquet, C. M.; Robert, F.; Morato, F.; Lippens, P.-E.; Olivier-Fourcade, J. *J. Power Sources* **2007**, *174*, 1091–1094.
(26) Jeitschko, W.; Jaberg, B. *Acta Crystallogr.* **1982**, *B 38*, 598.
(27) Lippens, P.-E.; Olivier-Fourcade, J.; Jumas, J.-C. *Hyperfine Interact.* **2000**, *126*, 137.
(28) Naille, S.; Lippens, P.-E.; Morato, F.; Olivier-Fourcade, J. *Hyperfine Interact.* **2006**, *167*, 785.

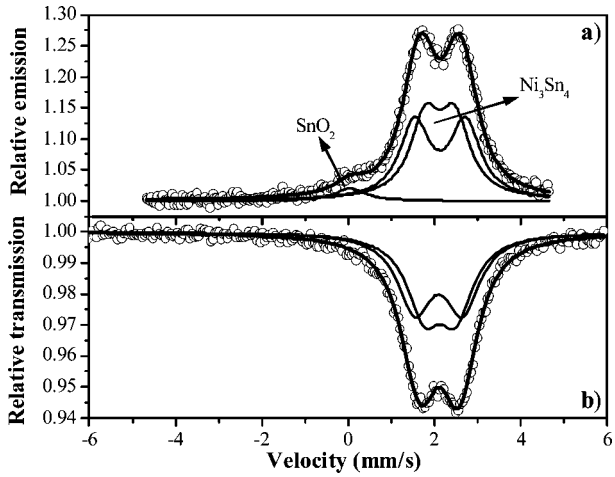

Figure 2. ^{119}Sn Mössbauer spectra of Ni_3Sn_4 at room temperature: (a) CEMS, (b) TMS.

Table 1. Hyperfine Parameters of ^{119}Sn Mössbauer Spectra Shown in Figure 2: δ (isomer shift relative to $BaSnO_3$), Δ (quadrupole splitting), and Relative Area (%)

		TMS			CEMS		
		δ (mm/s)	Δ (mm/s)	%	δ (mm/s)	Δ (mm/s)	%
Ni_3Sn_4	site 1	2.01 (4)	0.70 (6)	50	2.02 (4)	0.68 (5)	48
	site 2	2.02 (4)	1.18 (6)	50	2.02 (4)	1.18 (5)	48
SnO_2					−0.06 (4)	0	4

was detected in the bulk of the synthesized material from the transmission spectrum, and this shows that the surface is rather sensitive to oxygen.

The XPS Ni $2p_{3/2}$ and Sn $3d_{5/2}$ core peaks and valence spectrum of synthesized Ni_3Sn_4 are shown in Figure 3. The relevant binding energies and atomic percentages are reported in Table 2. The Ni $2p_{3/2}$ core peak displays three components. The first one observed at 852.2 eV is attributed to metallic nickel of Ni_3Sn_4. The two other small components at 855.3 and 860.5 eV are the main line and the satellite peak of nickel oxide NiO and account for 14% of the Ni $2p_{3/2}$ signal. Since the analysis depth of XPS is about 5 nm, this result displays the oxidation of nickel at the very surface of the synthesized compound.

The Sn $3d_{5/2}$ core peak consists of two components. The first one at 484.9 eV is assigned to metallic tin of Ni_3Sn_4. The other one at 486.8 eV shows the presence of tin oxide (SnO_2) at the very surface of the sample. This confirms the results of CEMS, but here the relative proportion of tin oxide is much higher (53% of the signal instead of 4%) because the analysis depth of XPS is 5 nm instead of more than 100 nm for CEMS. It is worth noting that the relative proportion of oxide is higher for tin than for nickel. Moreover, the Sn/Ni ratio measured by XPS is higher than expected for Ni_3Sn_4 (4.9 instead of 1.33). This is certainly due to the higher oxygen affinity of tin and explains why tin segregates to the surface. Therefore, most of the surface consists of SnO_2. This might have an influence on the surface properties of this material and its reactivity toward the electrolyte in a Li-ion battery.

The valence spectrum of the sample displays an intense signal at 23−28 eV and a weak hump at 0−13 eV. The narrow and intense peaks at 23.9 and 24.9 eV are the Sn

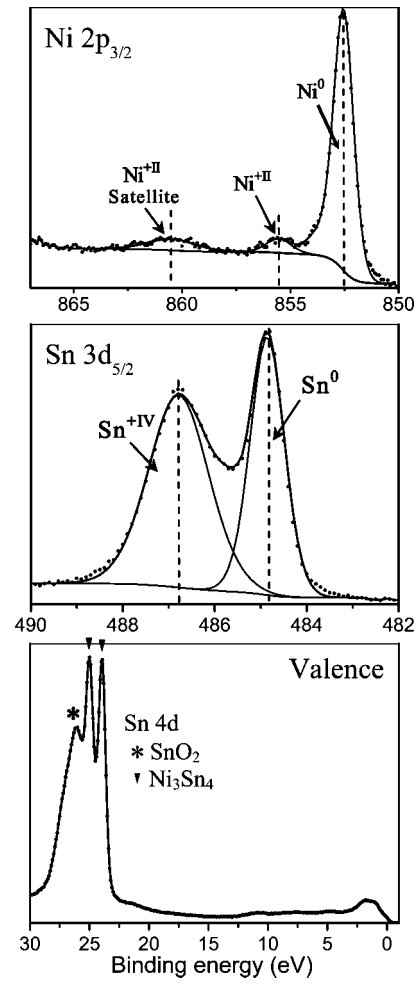

Figure 3. XPS Ni $2p_{3/2}$ and Sn $3d_{5/2}$ core peaks and valence spectrum of Ni_3Sn_4.

Table 2. Binding Energies (eV) and Atomic Percentages (%) of Elements Ni, Sn, O, and C from XPS Spectra of Synthesized Ni_3Sn_4

	Ni_3Sn_4	
	B.E. (eV)	%
Ni $2p_{3/2}$	852.5	5.1
	855.3 + sat.	0.8
Sn $3d_{5/2}$	484.9	13.5
	486.8	15.2
O 1s	530.7	21.4
	532.2	13.2
C 1s	285.0	24.5
	286.4	4.5
	288.8	1.8

$4d_{5/2}$ and $4d_{3/2}$ components of Ni_3Sn_4, and the wide asymmetrical peak at 26 eV corresponds to the same components of SnO_2. According to electronic structure calculations (not shown here) the first peak at 2 eV can be attributed to Ni_3Sn_4 and the 4−13 eV weak components can be attributed to both Ni_3Sn_4 and SnO_2 valence bands.

3.2. Study of the First Electrochemical Cycle. Figure 4 shows the first galvanostatic discharge/charge cycle of a Li/Ni_3Sn_4 electrochemical cell. Upon discharge Ni_3Sn_4 reacts with 12.5 lithium, corresponding to a capacity of 515 (mA h)/g (4336 (mA h)/cm^3), and upon charge 6.8 lithium are restored, corresponding to a reversible capacity of 282 (mA h)/g (2374 (mA h)/cm^3). Points A−E of discharge (x = 0, 2, 4, 7, and 12.5 Li) and points F, G of charge (x = 8.6 and

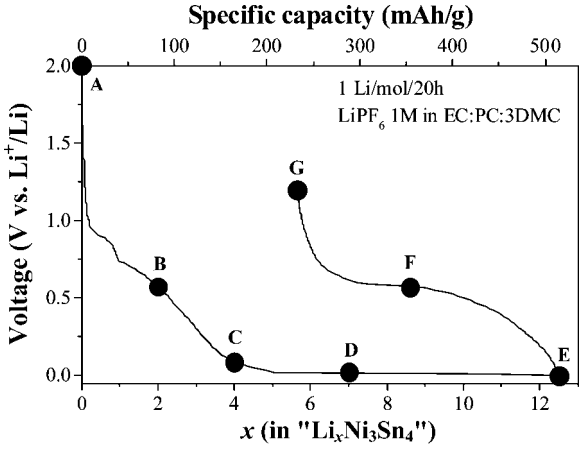

Figure 4. First discharge/charge cycle of a Li/Ni_3Sn_4 cell.

5.7 Li) correspond to the samples analyzed by XPS and ^{119}Sn Mössbauer spectroscopy. Point A corresponds to a Ni_3Sn_4 electrode simply soaked for 24 h in the electrolyte and then rinsed with the solvent DMC.

The discharge curve displays two distinct parts. First, from A to C ($x = 4$ Li), we can observe a voltage drop. This stage is generally attributed to the reduction of the surface oxide layer by lithium.[16,29,30] Then it is followed by a voltage plateau from C to E ($x = 12.5$ Li) corresponding to the Li_xSn alloying process. However, some doubts still remain concerning the interpretation of this discharge curve. Indeed, as shown by XPS the oxide layer is very thin (<5 nm). Since the average particle size is around 10 μm the oxide accounts for a very small part of the electrode material and it cannot explain the reaction of 4 mol of lithium per mole of Ni_3Sn_4. This consumption of 4 Li could be due either to the beginning of the Li−Sn alloying process or to the formation of the electrode/electrolyte interface (SEI). Unfortunately X-ray diffraction could not provide any information about the Li−Sn alloying reaction. Indeed, upon the whole cycle it could only show the amorphization of the Ni_3Sn_4 phase, but no diffraction peak of the electrode could be assigned to any Li−Sn alloy, probably due to nanocrystalline or amorphous phases. Note that previous works on other tin-based intermetallics have shown that Li−Sn nanoparticles are produced during reaction with lithium.[8,31] Therefore, Li−Sn nanoparticles are also expected in our case. To get a better insight of the mechanisms occurring upon the first discharge/charge cycle, we carried out Mössbauer and XPS experiments.

3.2.1. ^{119}Sn Mössbauer Spectroscopy. As shown in Figure 5, no change in the Mössbauer spectra of the Ni_3Sn_4 electrode could be observed up to 4 Li. For samples A and C, the spectra consist of the two doublets characteristic of Ni_3Sn_4. This result shows that no electron transfer mechanism involving Sn occurs in the bulk up to 4 Li.

After complete discharge at $x = 12.5$ Li (sample E), an additional contribution appears that can be fitted by two doublets of equal intensity with $\delta = 1.88(4)$ and 1.96(3) mm/s and $\Delta = 0.28(4)$ and 1.10(3) mm/s respectively, showing the formation of a new metallic phase. Several Li_xSn alloys can be found in the lithium−tin phase diagram, as said above. Some authors have proposed a reaction mechanism of lithium with Ni_3Sn_4 leading to the lithium-richest phase $Li_{22}Sn_5$.[18] However, these Mössbauer parameters are very close to those reported for Li_7Sn_2 and significantly different from those reported for other Li_xSn alloys.[6] This result unambiguously proves the formation of Li_7Sn_2 and excludes the formation of $Li_{22}Sn_5$. Thus, the proposed mechanism is the following:

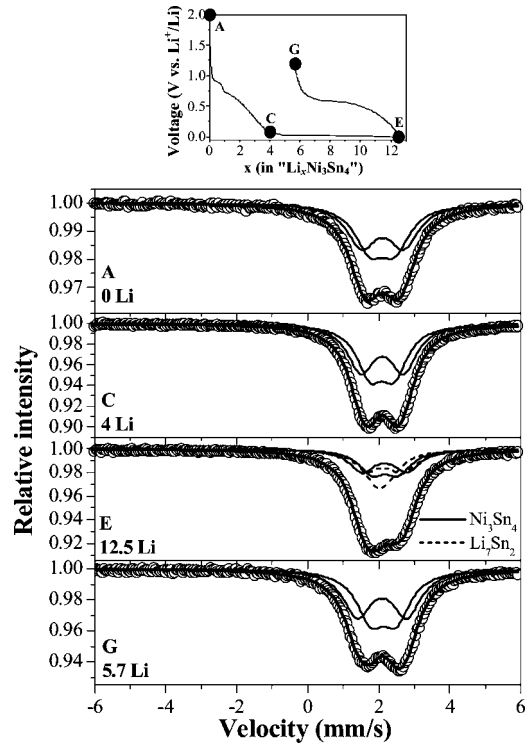

Figure 5. Room temperature ^{119}Sn Mössbauer spectra of the Ni_3Sn_4 electrode at different steps of the first cycle.

$$Ni_3Sn_4 + 14Li^+ + 14\,e^- \rightarrow 3Ni + 2Li_7Sn_2 \qquad (4)$$

Moreover, we can deduce from the Mössbauer spectrum of sample E that this reaction is not complete at the end of discharge, since 48% of the signal is still attributed to Ni_3Sn_4 (certainly due to kinetic limitations). This gives about 40% of tin atoms belonging to the Ni_3Sn_4 phase if we consider the same ratio of the recoil-free factors for Ni_3Sn_4 and Li_7Sn_2 as that obtained for $CoSn_2$.[14] From a quantitative point of view, taking into account that up to $x = 4$ Li no electron transfer concerns Ni_3Sn_4, only 8.5 Li are consumed to form the Li−Sn alloy at the end of discharge ($x = 12.5$ Li). Since 14 Li are necessary to complete reaction 4, the proportion of tin atoms remaining in unreacted Ni_3Sn_4 for 8.5 Li corresponds to 39%, in good agreement with the result obtained from the Mössbauer experiments.

At the end of charge (sample G), the spectrum is very close to that of starting Ni_3Sn_4, with similar hyperfine parameters. However, a weak asymmetry can be observed, which could be due to the presence of the β-Sn phase. Indeed, β-Sn is characterized by a narrow peak at $\delta = 2.56$ mm/s. Moreover, the recoilless factor of β-Sn at room temperature

(29) Benedek, R.; Thackeray, M. M. *J. Power Sources* **2002**, *110*, 406–411.
(30) Wolfenstine, J.; Campos, S.; Foster, D.; Read, J.; Behl, W. K. *J. Power Sources* **2002**, *109*, 230–233.
(31) Xue, M.-Z.; Fu, Z.-W. *Solid State Ionics* **2006**, *177*, 1501–1507.

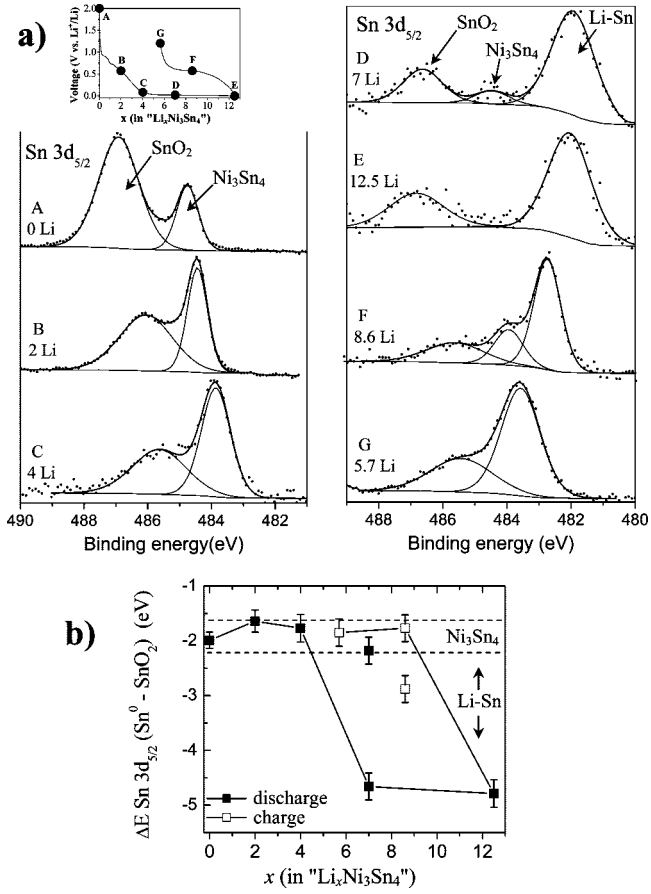

Figure 6. Sn $3d_{5/2}$ XPS of the Ni_3Sn_4 electrode at different steps of the first cycle: (a) spectra, (b) binding energy difference between the oxide and the metal.

is very weak ($f = 0.045$)[32] so that a weak asymmetry in this spectrum at room temperature could result from a non-negligible amount of β-Sn in the sample. Therefore, we recorded the Mössbauer spectrum at 75 K (not shown here). This lower temperature did not modify the shape of the spectrum, and so the presence of β-Sn in the sample can be excluded. This result allows rejecting the hypothesis that the alloying process is not reversible and that metallic tin is formed during charge ($Li_7Sn_2 \rightarrow 2\beta\text{-Sn} + 7Li^+ + 2e^-$). The weak asymmetry may result from the slightly disordered structure of the reformed nanosized Ni_3Sn_4. We can thus affirm that mechanism 4 is reversible during charge.

As a summary, this Mössbauer study displays the Li−Sn alloying process in the second stage of discharge between 4 and 12.5 Li. It shows also that no electron transfer mechanism involving Sn occurs from $x = 0$ to 4 Li. Thus another explanation has to be found for the consumption of 4 Li in the first stage of discharge. It could be due to side reactions at the electrode/electrolyte interface, and so XPS analyses of the electrode's surface will provide additional information.

3.2.2. XPS. Sn $3d_{5/2}$ core peaks of the Ni_3Sn_4 electrode at the different electrochemical steps are reported in Figure 6. The corresponding binding energies and atomic percentages are reported in Table 3. As for the pristine material, the Sn $3d_{5/2}$ spectrum of sample A (soaked electrode) consists of two peaks that can be attributed to Sn(IV) oxide and Sn(0) metal. The only difference with respect to the pristine Ni_3Sn_4 powder is that the oxide component (486.9 eV) is more intense, due to electrode manufacturing and contact with the electrolyte. During the first part of the discharge up to 4 Li (from A to C) we can observe a strong decrease of the oxide component. This decrease is much weaker during the second part of the discharge (points D and E). This is in good agreement with the conclusions of previous studies assuming that the reduction of surface oxide mainly occurs at the beginning of discharge.[29] This reduction process can be written as follows:

$$SnO_2 + 4Li^+ + 4e^- \rightarrow \beta\text{-Sn} + 2Li_2O \qquad (5)$$

Moreover, the relative proportion of oxide still remains the minority during charge (points F and G). This is in good agreement with previous works that concluded that this reduction process is not reversible (because it occurs only at the first cycle).[33]

The second important point to notice is the shift of the metallic tin Sn $3d_{5/2}$ component toward lower binding energies during discharge. The observation of this shift in Figure 6 a) is hindered by a global shift of the whole Sn $3d_{5/2}$ signal due to a differential charging effect during the XPS experiment between the conducting active material and the insulating compounds of the electrode (PTFE for example). Therefore, the difference between the binding energies of the metallic component(s) and the oxide component $\Delta E_{Sn3d5/2}$ (Sn^0-SnO_2) has been plotted in Figure 6 b, in order to provide a clearer evidence of this shift. We can see in this figure that, for up to 4 Li during discharge, the metallic component of Ni_3Sn_4 is not shifted with respect to the oxide component. This means that the alloying process has not started at this stage. Then in the second part of discharge (7 and 12.5 Li), this component is strongly shifted by 3 eV toward lower binding energies. This shift can be explained by the formation of the Li_7Sn_2 alloy according to mechanism 4. The absence of a gradual energy shift between 7 and 12.5 Li clearly indicates that no other Li_xSn compounds than Li_7Sn_2 were formed during the lithiation. All these results are consistent with our ^{119}Sn Mössbauer measurements.

The presence of a remaining weak component assigned to Ni_3Sn_4 in sample D shows that the reaction is not complete after $x = 7$ Li. Finally, at the end of discharge ($x = 12.5$ Li), the Ni_3Sn_4 component is barely visible and the two main components are due to SnO_2 and Li_7Sn_2, showing that the alloying reaction is almost complete. It is worth noting that Mössbauer experiments showed that a large amount of Ni_3Sn_4 still remained at the end of discharge. This difference between both techniques has to be explained. Since X-ray diffraction results let us assume that Li_xSn nanoparticles are formed upon discharge, no difference is expected between "surface" and "bulk" of the samples. However, some authors have shown that during reaction of lithium with tin-based intermetallics, the starting micrometric scale particles are disintegrated into a mosaic of nanoparticles, but during this process the overall shape of the starting particles is preserved

(32) Bahgat, A. A. *Phys. Status Solidi B* **1980**, *97*, K129.

(33) Courtney, I. A.; Dahn, J. R. *J. Electrochem. Soc.* **1997**, *144*, 2045–2052; 2943−2948.

Table 3. Binding energies (eV) and Atomic Percentages (%) of Elements Ni, Sn, F, O, C, and Li from XPS Spectra of the Ni_3Sn_4 Electrode during the First Cycle

	A soaked electrode 0 Li		B discharge 2 Li		C discharge 4 Li		D discharge 7 Li		E end of discharge 12.5 Li		F half-charge 8.6 Li		G end of charge 5.7 Li	
	B.E.	%	B.E.	%	B.E.	%	B.E.	%	B.E.	%	B.E.	%	B.E.	%
Ni 3p	66.6	0.6	66.5	0.5		*a*		*a*		*a*	64.7	0.1	65.9	0.1
Sn $3d_{5/2}$							481.9	0.02	482.0	0.02	482.7	0.1		
	484.8	1.0	484.4	0.7	483.9	0.08	484.5	0.003			483.9	0,03	483.6	0.2
	486.9	2.8	486.1	1.0	485.6	0.06	486.6	0.01	486.8	0.01	485.6	0.03	485.4	0.1
F 1s	684.9	0.5	685.0	1.2	684.9	2.3	684.9	2.4	685.0	1.5	684.9	3.1	684.9	3.6
	687.0	0.3					687.0	0.8	687.1	0.7			687.3	0.8
	689.1	8.2	689.3	17.4	689.4	12.3	689.6	10.3	689.6	10	689.5	6.1	689.4	14.8
O 1s							528.3	0.3	528.4	0.3	528.2	0.9		
	530.9	4.4	529.7	0.7	530.3	0.8					530.5	2.0	530.7	2.8
	532.0	1.7	531.9	20.6	531.8	22.3	531.9	17.1	531.9	19.8	531.8	23.4	531.9	17.4
	533.6	0.4	533.4	2.0	533.5	2.8	533.9	6.0	534.1	8.1	533.8	1.9	533.7	3.2
C 1s	284.3	76	284.0	12.8	283.6	4.0		*a*		*a*	283.5	5.1	283.5	7.1
			285.0	15.8	285.0	21.9	285.0	28.5	285.1	24.9	285.0	23.9	285.0	15
			286.6	3.1	286.5	5.5	286.8	7.4	287.1	7.5	286.5	4.2	286.6	7.2
			289.1	2.0	288.9	1.6	288.7	3.3	288.7	3.0	288.7	2.1	288.9	2.0
			290.2	5.7	290.2	6.0	290.3	4.0	290.3	4.4	290.1	5.6	290.3	5.6
	291.9	4.1	292.3	6.5	292.5	4.3	292.5	3.8	292.5	3.8	292.5	1.8	292.4	5.3
Li 1s							54.1	1.4	54.0	1.3	54.0	2.0	54.0	0.8
			55.9	10.0	55.7	16.1	55.8	14.7	55.8	14.7	55.7	17.7	55.8	14

[a] Below the limit of detection.

despite the volume expansion.[8] Therefore comparison between XPS and Mössbauer results lets us assume that the Li−Sn alloying process is complete at the surface of the former particles, while a non-negligible proportion of Ni_3Sn_4 still remains unreacted in the bulk.

During charge (points F and G) we observe a reincrease of the binding energy of the metallic component to recover the value of Ni_3Sn_4. At the end of charge (5.7 Li) only one metallic component assigned to Ni_3Sn_4 is present in the spectrum. At half-charge (8.6 Li) the Sn $3d_{5/2}$ spectrum still displays a third component attributed to a Li_xSn alloy. However, as we can see in Figure 6 b, its binding energy with respect to the oxide component is very different from that of Li_7Sn_2. This result lets us assume that a lithium-poorer alloy is formed upon charge at the surface of the Li_7Sn_2 particles and that this resulting tin-rich surface reacts with nickel to reform Ni_3Sn_4.

Other information can be provided by the tin atomic percentage measured by XPS at the surface of the Ni_3Sn_4 electrode upon the first discharge/charge cycle, as shown in Figure 7. The tin atomic percentage measured before the electrochemical reaction is only 3.8% due to the presence of PTFE binder and carbon black conductive additive in the electrode. Upon discharge, this amount decreases dramatically to reach very weak values about 0.03% (note that it is possible here to measure such small atomic percentages of tin due to the very high cross section of the Sn $3d_{5/2}$ core peak). Most of this decrease occurs at the beginning of discharge between 0 and 4 Li. In the second part of discharge this decrease becomes negligible. As we can see in Figure 7, the same phenomenon is observed for the atomic percentage of carbon black, which decreases from 76% before discharge (due to its high specific surface area) down to 4% after 4 Li. This strong decrease results from the formation of a SEI that covers the surface of the particles in the electrode. This covering concerns both the active material Ni_3Sn_4 and the carbon conductive additive. It does not concern the polymer binder, the amount of which stays

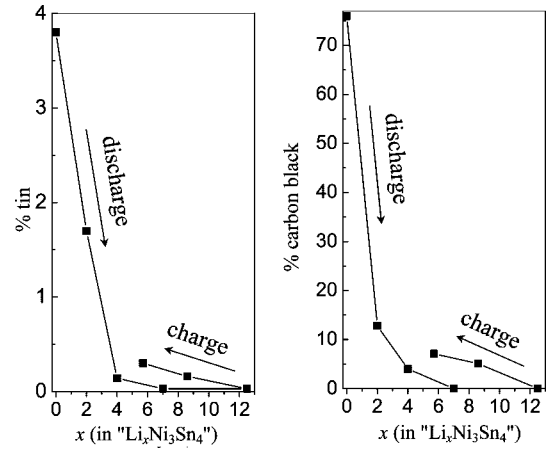

Figure 7. Atomic % of tin and carbon black measured by XPS at the surface of the Ni_3Sn_4 electrode.

between 12 and 24% upon discharge. This shows that the formation of the SEI is linked to the electrochemical process. This covering occurs mainly during the first stage of the discharge between 0 and 4 Li, and it is irreversible since the atomic percentages of tin and carbon reincrease only weakly upon charge. So this phenomenon allows us to explain the particular shape of the discharge curve of Figure 4. The voltage drop observed between 0 and 4 Li weakly results from the reduction of surface tin oxide and mainly from the formation of the electrode/electrolyte interface. This is the reason why no electronic transfer mechanism concerns the active material Ni_3Sn_4 between 0 and 4 Li. Ni 3p and Li 1s core peaks of the Ni_3Sn_4 electrode at the different electrochemical steps are reported in Figure 8 a. In these spectra Ni 3p (66 eV) is the signature of the active material (note that, due to the presence of fluorine in these samples, the Ni 2p core peak at 852 eV is hidden by the F $K\,L_1\,L_{23}$ Auger peak). The decrease of the Ni 3p peak and its disappearance after 4 Li confirms the covering process of the alloy particles by the SEI in the first stage of discharge.

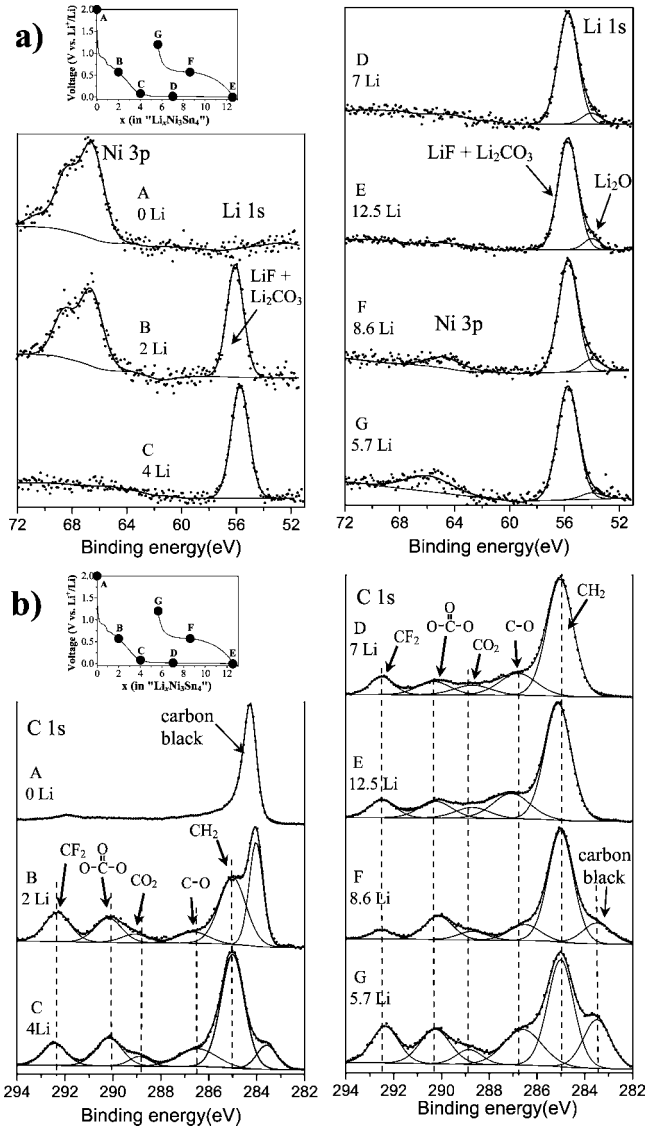

Figure 8. (a) Ni 3p, Li 1s, and (b) C 1s XPS of the Ni_3Sn_4 electrode at different steps of the first cycle.

The irreversibility of this process is also confirmed here, since the Ni 3p peak is hardly detectable at the end of charge.

The Li 1s peak results from a mixture of lithiated compounds formed in the surface layer. It mainly consists of LiF and Li_2CO_3, as we will see from C 1s and F 1s core peaks. Both compounds have very close binding energies (56 and 55.5 eV, respectively) and cannot be distinguished in the spectra. The absence of any Li 1s peak for sample A (Ni_3Sn_4 electrode simply soaked 24 h in the electrolyte and then rinsed with the solvent DMC) means that no lithiated compounds and thus no SEI layer was formed after simple contact of the electrode with the electrolyte. Thus, the formation of this passivation layer is an electrochemically driven process. Finally, in several spectra we can also notice the signature of Li_2O at 54 eV, which results from the reduction of surface tin oxide.

The C 1s core peaks are reported in Figure 8 b. The spectrum of sample A ($x = 0$ Li) consists of one narrow peak at 284.3 eV from carbon black and of another weak component at 292 eV from PTFE binder $(-CF_2-CF_2-)_n$. No peak relating to any kind of surface layer can be detected at this stage. Then upon discharge we can observe the strong decrease of the carbon black component that totally disappears after 7 Li due to covering by a passivation layer, as said above. After $x = 2$ Li the spectrum displays a completely different shape, and this shape is kept almost unchanged from 4 Li to the end of the cycle. The peak at 292 eV relating to PTFE is still observed during the whole cycle, since the binder is not (or very weakly) covered by the passivating layer. Four new components appear at 285, 286−287, 289, and 290 eV corresponding to the carbon atoms in CH_2, C−O, O=C−O, and CO_3-like environments, respectively. The appearance of these new components displays the formation of organic species resulting from the degradation of the electrolyte solvents at the surface of the electrode. The peak at 285 eV can be assigned to hydrocarbon contamination always observed at the surface of the samples but also to possible hydrocarbon species formed in the SEI. A detailed identification of the species making up the electrode/electrolyte interface can be very difficult. Many works have been carried out on graphite and carbonaceous negative electrodes in order to shed light on these phenomena.[2,34–37] Several mechanisms have been proposed to explain the formation of Li_2CO_3 and $ROCO_2Li$ by a reduction process (mono- or bielectronic) of the electrolyte solvents:

$$\text{DMC:}\quad CH_3OCO_2CH_3 + 2e^- + 2Li^+ \rightarrow Li_2CO_3 + C_2H_6(g) \tag{6}$$

$$\text{EC:}\quad (CH_2O)_2CO + 2e^- + 2Li^+ \rightarrow Li_2CO_3 + C_2H_4(g) \tag{7}$$

$$\text{DMC:}\quad 2CH_3OCO_2CH_3 + 2e^- + 2Li^+ \rightarrow 2CH_3OCO_2Li + C_2H_6(g) \tag{8}$$

These mechanisms may also occur at the surface of a Ni_3Sn_4 electrode and may concern any of the three solvents used in our case (EC, PC, DMC) and lead to the formation of lithium carbonate Li_2CO_3 and/or lithium alkyl carbonates $ROCO_2Li$. The appearance of a CO_3 component in the C 1s spectra is the signature of such carbonated species. The peak at 286−287 eV (carbon atoms in one-oxygen environment) can be explained in several ways. First it could be due to the same lithium alkyl carbonates species $ROCO_2Li$ (CH_3OCO_2Li, for example). However, it could be attributed to other organic species formed with other mechanisms, as, for example, polymerization of EC by ring-opening leading to poly(ethylene oxide) PEO oligomers:[38,39]

(34) Aurbach, D.; Daroux, M. L.; Faguy, P. W.; Yeager, E. *J. Electrochem. Soc.* **1987**, *134*, 1611–1620.
(35) Andersson, A. M.; Edström, K. *J. Electrochem. Soc.* **2001**, *148*, A1100–A1109.
(36) Augustsson, A.; Herstedt, M.; Guo, J.-H.; Edstr̈om, K.; Zhuang, G. V.; Ross, P. N.; Rubensson, J.-E.; Nordgren, J. *Phys. Chem. Chem. Phys.* **2004**, *6*, 4185–4189.
(37) Verdier, S.; El Ouatani, L.; Dedryvère, R.; Bonhomme, F.; Biensan, P.; Gonbeau, D. *J. Electrochem. Soc.* **2007**, *154*, A1088–A1099.
(38) Laruelle, S.; Pilard, S.; Guenot, P.; Grugeon, S.; Tarascon, J.-M. *J. Electrochem. Soc.* **2004**, *151*, A1202–A1209.
(39) Vogdanis, L.; Martens, B.; Uchtmann, H.; Hensel, F.; Heitz, W. *Makromol. Chem.* **1990**, *191*, 465–472.

$$\text{EC:}\quad n(CH_2O)_2CO \rightarrow (-CH_2-CH_2-O-)_n + nCO_2 \tag{9}$$

In particular, the presence of CO_2 gas dissolved in the electrolyte of Li-ion batteries is a well-known phenomenon.[40] The formation of lithium alcoholates ROLi in the electrode/electrolyte interface has also been mentioned.[36]

The last C 1s peak at 289 eV (carbon atoms in two-oxygen environment) can also be explained in several ways. Some authors have mentioned the formation of RCO_2Li species.[41] Another mechanism discussed in a previous work consists in the reduction of carbon dioxide, CO_2, dissolved in the electrolyte leading to the formation of oxalates.[36,38,42] As a result the composition of the electrode/electrolyte interface appears as a complex mixture, and only a few compounds can be unambiguously identified after analysis of all XPS spectra. However, the overall shape of the C 1s spectrum still remains almost unchanged from 2 Li to the end of the discharge and even to the end of the cycle, and so the composition of the SEI layer looks rather stable during the whole electrochemical cycle.

The O 1s core peaks are reported in Figure 9a. The spectrum of sample A consists of one peak at 530.9 eV assigned to surface oxide SnO_2 and of two additional peaks attributed to oxygenated species forming in small quantities at the surface of the Ni_3Sn_4 electrode following its contact with the electrolyte. After 2 Li during discharge the peak relating to SnO_2 is barely detectable, and it disappears totally after 4 Li, in good agreement with the reduction process of surface tin oxide. After 2 Li and up to the end of the cycle the spectrum is dominated by a main peak at 531.9 eV which is characteristic for carbonate species. Spectra B and C (2 and 4 Li) display the typical asymmetrical shape of Li_2CO_3.[43] In the second part of discharge (7 and 12.5 Li) a shoulder is observed at 534 eV. This binding energy is significantly higher than the value expected for the shoulder observed in lithium alkyl carbonates $ROCO_2Li$ (533.3 eV).[43] It is the same value as the main O 1s peak of polycarbonates[44] and could be the signature of a small amount of these polycarbonates. But it is difficult to conclude on the exact composition of the interface. Finally, we can notice in several spectra the signature of Li_2O at 54 eV, which results from the reduction of surface tin oxide, in good agreement with the same observation in Li 1s spectra.

The F 1s spectra reported in Figure 9b consist of three peaks at 685, 687, and 689 eV, corresponding to LiF, $LiPF_6$, and PTFE binder, respectively. The peak assigned to $LiPF_6$ is very weak and sometimes not detectable, due to the very low amount of salt remaining at the surface of the electrode after washing with DMC solvent (and the XPS peaks relating to P element were under the detection limit for all samples).

The F 1s peak assigned to PTFE $(-CF_2-CF_2-)_n$ shows a great intensity during the whole cycle since the binder is not (or very weakly) covered by the passivation layer, as said above. LiF is a degradation product of the salt $LiPF_6$, and it is commonly detected at the surface of positive or negative electrodes of lithium-ion batteries. The peak assigned to this compound presents a fluctuating intensity and displays no clear evolution during the discharge/charge cycle. The amount of LiF ranges from 1% to 7% at the surface of the electrode. Several mechanisms have been proposed to explain the deposition of LiF ensuing from the reaction of $LiPF_6$ with traces of water in the electrolyte or with other degradation compounds formed during the electrochemical cycle such as Li_2CO_3.[45–47]

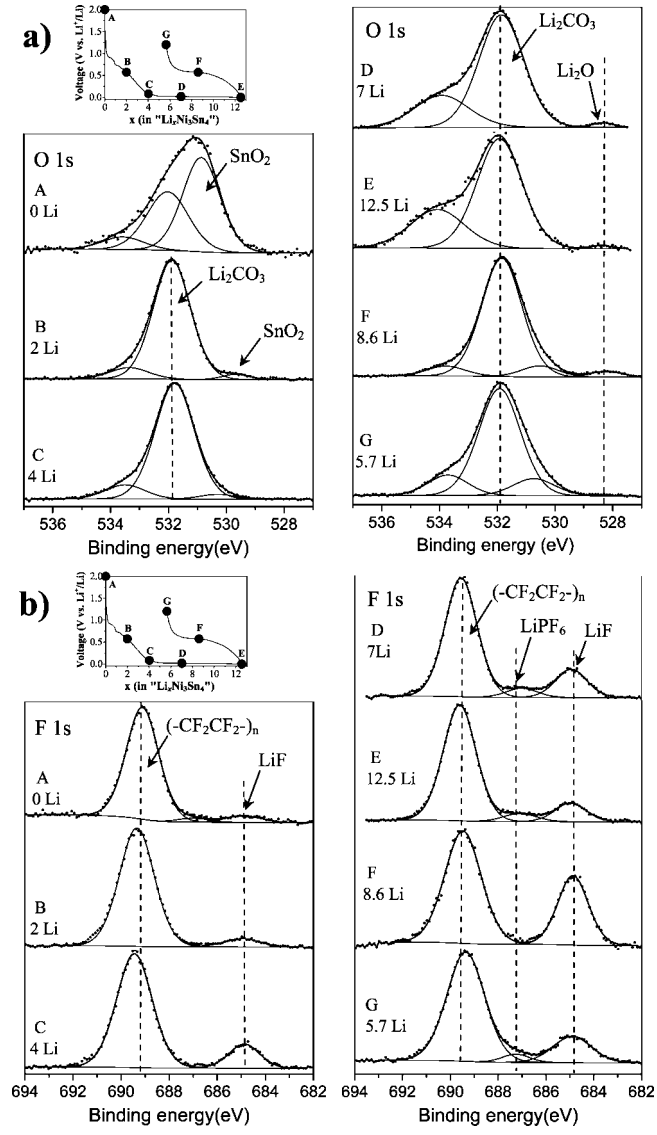

Figure 9. (a) O 1s and (b) F 1s XPS of the Ni_3Sn_4 electrode at different steps of the first cycle.

$$LiPF_6 + H_2O \rightarrow LiF + POF_3 + 2HF \tag{10}$$

$$LiPF_6 + Li_2CO_3 \rightarrow 3LiF + POF_3 + CO_2 \tag{11}$$

(40) Xu, Y. *Chem. Rev.* **2004**, *104*, 4303–4418.
(41) Zhang, S. S. *J. Power Sources* **2006**, *162*, 1379–1394.
(42) Dedryvère, R.; Laruelle, S.; Grugeon, S.; Gireaud, L.; Tarascon, J.-M.; Gonbeau, D. *J. Electrochem. Soc.* **2005**, *152*, A689–A696.
(43) Dedryvère, R.; Gireaud, L.; Grugeon, S.; Laruelle, S.; Tarascon, J.-M.; Gonbeau, D. *J. Phys. Chem. B* **2005**, *109*, 15868–15875.
(44) Beamson, G.; Briggs, D. *High resolution XPS of organic polymers: the Scienta ESCA300 database*; Chichester, 1992.
(45) Aurbach, D.; Markovsky, B.; Weissman, I.; Levi, E.; Ein-Eli, Y. *Electrochim. Acta* **1999**, *45*, 67.
(46) Gireaud, L.; Grugeon, S.; Pilard, S.; Guenot, P.; Tarascon, J.-M.; Laruelle, S. *Anal. Chem.* **2006**, *78*, 3688–3698.
(47) Vetter, J.; Novák, P.; Wagner, M. R.; Veit, C.; Möller, K.-C.; Besenhard, J. O.; Winter, M.; Wohlfahrt-Mehrens, M.; Vogler, C.; Hammouche, A. *J. Power Sources* **2005**, *147*, 269–281.

$$LiPF_6 + 4ROLi \rightarrow (RO)_4PF + 5LiF \rightarrow OP(OR)_3 + RF + 5LiF \quad (12)$$

These mechanisms lead to the formation of phosphates or fluorophosphates that are also commonly detected at electrode/electrolyte interfaces. However, in our case no phosphorus-containing compounds could be detected. This may be due to their solubility in DMC solvent used for washing the electrodes before XPS analysis. However, we could detect these species on graphite in previous works, despite washing the electrodes with DMC.[37,48] Therefore, the absence of phosphates and fluorophosphates at the surface of our samples could be due to the structure of the SEI. These species could be mixed for example with other organic compounds, which are soluble in DMC, and consequently could be removed during washing.

In order to complete the study of the SEI layer composition, we decided to analyze the XPS valence spectra. Interestingly, while XPS core peaks are commonly exploited, valence spectra are very rarely used in this kind of study. The reason is that valence spectra of electrode surfaces are often very difficult to interpret after electrochemical cycling, due to the complex mixtures of organic and inorganic species making up the interface, which all contribute to the valence spectrum. A detailed interpretation of a valence spectrum requires the help of calculations, as it is representative of the density of states of the occupied energy levels close to the Fermi level. However, it can be more easily used as a fingerprint to identify a compound (or a mixture of a few compounds), and it can provide additional information.

Valence spectra of the Ni_3Sn_4 electrode at the different electrochemical steps are reported in Figure 10. The spectrum of sample A (soaked electrode) is rather similar to that of the pristine Ni_3Sn_4 powder. The main difference is that the intensity of the Sn 4d component assigned to SnO_2 is higher, due to surface oxidation after electrode manufacturing and contact with the electrolyte, as said above. The absence of any additional peaks in the spectrum confirms that no surface layer has been formed after simple contact of the electrode with the electrolyte.

At the beginning of discharge ($x = 2$ Li) we can observe a strong decrease of the SnO_2 component resulting from the above-mentioned reduction process (eq 5). Additional peaks appear in the spectrum, showing the formation of new compounds at the electrode/electrolyte interface. After 4 Li, the Sn 4d signal of the electrode active material has totally disappeared, following its covering by the SEI. Then, from this stage to the end of the discharge and to the end of the cycle, the valence spectrum retains the same overall shape, meaning that the composition of the interface does not significantly change. This valence shape is simple enough to be recognized. First, the narrow peak at about 30 eV can be identified as the main valence peak (F 2s) of LiF.[42] The smaller peak of LiF at 8 eV (F 2p) can also be detected in samples D and E. Second, the characteristic shape of Li_2CO_3 with a main asymmetrical peak at 24 eV and three other peaks at 13, 11, and 6 eV can be also recognized (the valence spectra of carbonate species Li_2CO_3 and $ROCO_2Li$ have been carefully analyzed in a previous work [43]). Therefore, the valence spectra of the electrode's surface roughly appears as a mixture of LiF and Li_2CO_3. This means that both compounds are the main products of the SEI and that other compounds are the minority. Taking this result into consideration, quantitative analysis from core peaks (Table 3) shows that LiF and Li_2CO_3 account for about 40% of the surface. Moreover, these spectra show that Li_2CO_3 is the main carbonate species because lithium alkyl carbonates $ROCO_2Li$ or polycarbonates display additional peaks in the 15−20 eV range, which are not observed here.

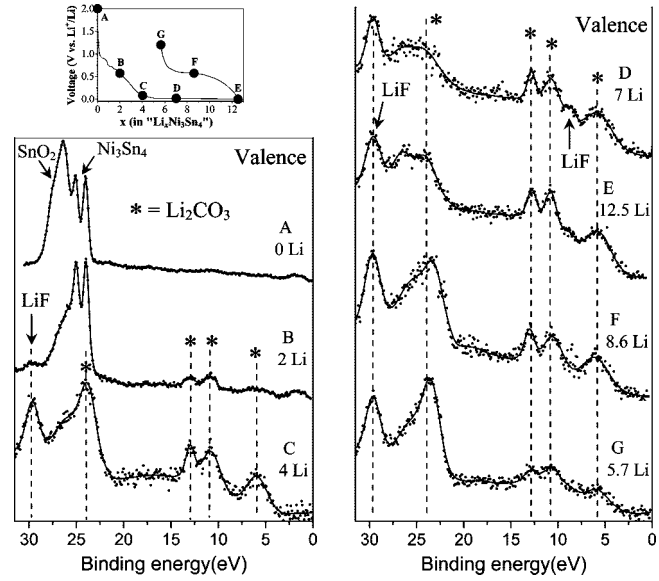

Figure 10. XPS valence spectra of the Ni_3Sn_4 electrode at different steps of the first cycle.

As a summary, this study shows that the formation of the SEI occurs in the first stage of discharge (between 0 and 4 Li), and that its thickness and composition change only weakly in the rest of the cycle. This result is rather different from that obtained by Edström and co-workers[20] with AlSb electrodes, for which the thickness of the SEI increases upon discharge and decreases upon charge. We still have to understand if this difference of behavior arises from the electrode nature or from different experimental conditions, which could have a great influence.

Finally, the composition of the SEI is rather close to that observed at the surface of a graphite electrode. However, the presence of phosphates or fluorophosphates cannot be detected as in the case of graphite. These species may be removed together with soluble products during electrode washing with DMC, and they cannot be detected according to our experimental conditions.

4. Conclusion

In this work, we have investigated the changes undergone by a Ni_3Sn_4 electrode during lithiation/delithiation in an electrochemical cell. This study allowed us to show that 4 mol of lithium per mole of Ni_3Sn_4 are consumed to form the SEI at the first stage of discharge. The Li−Sn alloying process occurs in the second stage of discharge and leads to

(48) Leroy, S.; Blanchard, F.; Dedryvère, R.; Martinez, H.; Carré, B.; Lemordant, D.; Gonbeau, D. *Surf. Interface Anal.* **2005**, *37*, 773–781.

the direct formation of Li_7Sn_2. This mechanism is reversible and allows restoring the Ni_3Sn_4 phase at the end of the first cycle.

XPS analyses showed that the thickness and composition of the SEI do not change upon charge, showing that its formation is not reversible. The formation mechanisms of the SEI and its composition seem to be close to those observed for a graphite electrode. In particular, no passivating layer exists after simple contact of the electrode with the electrolyte, and the SEI is formed in the same potential range as for a graphite electrode. As for a carbonaceous electrode the SEI layer mainly consists of Li_2CO_3 and LiF and to a lesser extent of oxygenated organic compounds.

Acknowledgment. Financial support by the ANR (Liban project) and the European Community (ALISTORE Network of Excellence) are gratefully acknowledged.

CM8006099